Effect of magnetic field quantization on the shallow acceptor spectrum in strained Ge/GeSi heterostructures

V. Ya. Aleshkin, V. I. Gavrilenko, and D. B. Veksler
Institute for Physics of Microstructures, Nizhny Novgorod GSP-105, 603950, Russia

L. Reggiani
INFM National Nanotechnology Laboratory, Dipartimento di Ingegneria dell' Innovazione, Universitá di Lecce, Via Arnesano s/n, I-73100 Lecce, Italy

(Received 24 February 2002; revised manuscript received 12 June 2002; published 31 October 2002)

We presents a calculation of acceptor energy states in Ge/GeSi heterostructures in the presence of a magnetic field performed within an effective mass approach. Both spatial quantization and the effect of the strain due to the mismatch between the Ge and GeSi layers have been accounted for. Together with energy states and wavefunctions we have calculated the matrix elements associated with the electromagnetic interaction in the dipole approximation. The results so obtained have provided the basis for a microscopic interpretation of photoresponse spectra as a function of the magnetic field up to 50 kOe, which were measured at 4.2 K. The theory is found to agree satisfactorily with experiments and has enabled us to obtain a close correlation between the photoresponse spectra and the spatial profile of the acceptor concentration inside the heterostructure.

DOI: 10.1103/PhysRevB.66.155336 PACS number(s): 73.21.Ac, 73.21.Fg, 73.50.Pz

I. INTRODUCTION

Strained heterostructures (HS's) based on Ge and Si are of considerable interest because of the wide range of physical properties which can be modeled through band structure engineering and then applied to advanced electronic devices. Here we focus our attention to the energy states of shallow impurity centers which control the photoconduction properties of the structure and can be conveniently used to develop photodetectors in the far and mid infrared range. From one hand, when compared with the ideal hydrogen like model of the bulk, it is known that size quantization in a multiple quantum-well (QW) heterostructure leads to a binding energy which (i) increases [for about a factor of 4 (Ref. 1)] when the impurity center is located at the center of the QW and (ii) decreases systematically when the impurity center is moved from the center of the QW to the center of the barrier. On the other hand, the valence band of Ge and Si is known to be degenerate at the Γ_8^+ point and to consist of light and heavy holes subbands. Biaxial stress of Ge layers (quantum well layers), due to the difference between the Ge and the GeSi alloy lattice constants, causes the splitting of the valence band and, as a consequence, a considerable decrease of the value of the effective mass at the top of the valence band. As a result, the acceptor binding energy is expected to decrease significantly. Accordingly, the opportunity is provided to engineer the energy spectra of shallow acceptors by varying compositional and structure parameters such as the widths of the Ge and alloy layers, the Si concentration in the alloy, etc. We further note that an external magnetic field aligned with the HS axis induces the quantization of carrier motion in the QW plane, splits the acceptor states, and imposes simple selection rules for the dipole optical transitions in the high field limit similar to the case of donors in bulk semiconductors.[2]

The theoretical description of shallow impurities in semiconductor structures is a major area of interest since many years.[3–8] Despite of that, an exact analytical solution of the Schrödinger equation for the donor (acceptor) state in the presence of a magnetic field, to our knowledge, is not available in the literature, and more or less approximate methods were generally used. To this purpose, many different approaches have been employed in both bulk and QW systems. Among them, the most common approaches make use of perturbation, variational, or adiabatic methods. A comprehensive review for bulk systems was made in Refs. 9, and 10. More recent investigations for the case of multi-QW systems can be found in Ref. 11 for donors and Ref. 12 for acceptors. However, the majority of the theoretical methods used so far meet with difficulties in providing reliable results on energies and wave functions of highly excited impurity states, such as metastable or so-called autoionization states.[13] Therefore, there is still an open interest in providing a rigorous theoretical framework able to include highly excited states.

The aim of the present work is to address this issue by developing a model for shallow acceptor impurities in multi-QW HS, and apply it to $Ge/Ge_{1-x}Si_x(111)$ HS where existing photoconductive experiments[14] can be microscopically interpreted. The method is based on the diagonalization of the total Hamiltonian of an acceptor impurity using as a basis set the eigenfunctions in the absence of the impurity potential. A similar technique has been used earlier to find the acceptor states in a Ge/GeSi(111) HS quantum well, but without including the presence of a magnetic field.[15] The calculations carried out in this work allow us to provide a rigorous description of energy states, wavefunctions, matrix element for optical transition, etc., as functions of magnetic field, location of the impurity center inside the HS elementary cell, intrinsic strain, and quantum confinement. The results will shed new light in the interpretation of the main

features observed in the photoconductivity spectra of undoped, with residual acceptors, Ge/GeSi multiple QW heterostructures.[14] The validation of the theoretical approach may prove useful in terms of developing further modeling of impurity photodetectors for the far and mid-IR ranges.

The content of the paper is summarized as follows. Section II presents the theoretical approach. Results are reported in Sec. III for the energy levels and the photoconductance. Major conclusions are drawn in Sec. IV.

II. THEORETICAL APPROACH

The physical system of interest is a multi-QW HS consisting of a large number (162 in the considered HS) of Ge/GeSi periods in the presence of a magnetic field applied in the direction of the structure growth. The elementary cell consists of a quantum well (Ge) followed by a quantum barrier (QB) (GeSi). The width of the barrier is sufficiently large to justify the decoupling of one elementary structure from the others. The whole width of the HS exceeds the critical value providing stress relaxation between the Ge substrate and the HS and, as a consequence, the elastic biaxial deformation of both the GeSi and Ge layers. The acceptor impurities are distributed randomly in the structure according to the undoped (with residual acceptor) configuration.[14] We remark that the x-ray investigations of these structures have showed that there is a single lattice constant of the superlattice different from that of the substrate.[16] Our main objective is to calculate the energy levels and the wave functions of an acceptor impurity located in a given position inside the elementary cell in the presence of a magnetic field and of an internal strain. Then, we aim at interpreting experimental results of photoconductivity spectra in the presence of a magnetic field. To this purpose we consider the electron motion in the Coulomb potential of the acceptor center in a strained QW HS in a magnetic field applied in the direction of structure growth (OZ axis $\|[111]$). Furthermore, charge effect at the heterointerface is negligible because the difference of dielectric constants at the heterointerface is small (less than 3%) due to the small Si content in the barrier (12%). The 4×4 Hamiltonian describing the motion of the electron $\|\hat{H}\|=\|\hat{H}_L\|+\|\hat{H}_d\|+\|\hat{H}_{\mathrm{QW}}\|+\hat{U}_q$ is taken as the sum of the following four terms: (i) the Luttinger Hamiltonian in a magnetic field,[17] (ii) the potential describing deformation effects,[18] (iii) the potential of a rectangular quantum well, (iv) the Coulomb potential. Without the latter term this Hamiltonian, as written for the envelope wave functions, has the form

$$\|\hat{H}_0\|=\frac{\hbar eH}{m_0c}\begin{Bmatrix} F_+ & H & I & 0 \\ H^+ & G_+ & 0 & I \\ I^+ & 0 & G_- & -H \\ 0 & I^+ & -H^+ & F_- \end{Bmatrix} \tag{1}$$

with the Hamiltonian elements given by

$$F_\pm=[\gamma_1(z)+\gamma_3(z)]\left(\hat{a}^+\hat{a}^-+\frac{1}{2}\right)+\frac{1}{2}\hat{\zeta}[\gamma_1(z)-2\gamma_3(z)]\hat{\zeta}$$
$$\pm\frac{3}{2}\kappa+\frac{m_0c}{\hbar eH}\left(\frac{d(z)}{\sqrt{3}}(\varepsilon_{xx}-\varepsilon_{zz})+V(z)\right),$$

$$G_\pm=[\gamma_1(z)-\gamma_3(z)]\left(\hat{a}^+\hat{a}^-+\frac{1}{2}\right)+\frac{1}{2}\hat{\zeta}[\gamma_1(z)+2\gamma_3(z)]\hat{\zeta}$$
$$\pm\frac{1}{2}\kappa-\frac{m_0c}{\hbar eH}\left(\frac{d(z)}{\sqrt{3}}(\varepsilon_{xx}-\varepsilon_{zz})+V(z)\right),$$

$$I=\sqrt{\frac{1}{3}}\left[[\gamma_2(z)+2\gamma_3(z)]\hat{a}^{-2}-2[\gamma_2(z)-\gamma_3(z)]\frac{1}{2}\{\hat{\zeta}\hat{a}^+\}\right],$$

$$H=-\sqrt{\frac{2}{3}}\left[[2\gamma_2(z)+\gamma_3(z)]\frac{1}{2}\{\hat{\zeta}\hat{a}^-\}-[\gamma_2(z)-\gamma_3(z)]\hat{a}^{+2}\right].$$

Here $\hat{\zeta}=\hat{k}_z\lambda$, with $\hat{k}_z$ the z component of the momentum operator, $\lambda=\sqrt{c\hbar/(eH)}$ is the magnetic length, e the modulus of the electron charge, H the magnetic field, c the light velocity, m_0 the free electron mass, and $V(z)$ the quantum well potential. Due to the layered structure the material specific parameters such as the Luttinger band parameters γ_1, γ_2, γ_3, κ,[19] deformation potential coupling constant $d(z)$, as well as the components of the deformation tensor $\varepsilon_{zz}(z)$, $\varepsilon_{xx}(z)$ ($OX\|[1\bar{1}0]$) depend on z:

$$\hat{a}^\pm=\frac{\lambda}{\sqrt{2}}\left[-i\frac{\partial}{\partial x}+\frac{e}{\hbar c}A_x\right]\pm i\frac{\lambda}{\sqrt{2}}\left[-i\frac{\partial}{\partial y}+\frac{e}{\hbar c}A_y\right]. \tag{2}$$

Here $\hat{a}^+$ is the creation and $\hat{a}^-$ the annihilation operators whose form is determined by the gauge of the vector potential $\vec{A}$. The expression $\{\hat{a}\hat{b}\}=1/2(\hat{a}\hat{b}+\hat{b}\hat{a})$ designates the anticommutator of operators in the brackets, and is here introduced to keep the Hamiltonian Hermitian at the boundary.[1] The fact that the Hamiltonian is Hermitian allows us to obtain the boundary conditions by integrating this Hamiltonian in the proximity of a heterointerface.

By detailing the model, we note that band and other parameters in the alloy are calculated using a linear interpolation from Ge to Si parameter values. Since the Si content in the structure under consideration does not exceed 12%, such an interpolation would not bring any significant difference with respect to more rigorous approaches.[20] Accordingly, taking x as the Si content in the alloy, it is $\gamma_1=-13.38(1-x)-4.22x$, $\gamma_2=-4.24(1-x)-0.39x$, $\gamma_3=-5.69(1-x)-1.44x$, and $\kappa=-3.24$, where bulk values are taken from Ref. 21. The deformation terms in the Ge layer of the QW and in the GeSi layer of the QB are accounted as follows:

$$\varepsilon_{xx}=a/a_0-1,\quad \varepsilon_{zz}=\frac{-2(c_{11}+2c_{12}-2c_{44})}{c_{11}+2c_{12}+4c_{44}}\varepsilon_{xx}, \tag{3}$$

where $a_0=5.65$ Å is the lattice constant of the unstrained Ge in the case of QW layer and a_0 (Å)$=5.65-0.24x(1-x)-0.22x^2$ is the lattice constant of the unstrained QB material. The argument a is the in-plain lattice constant of the full structure determined from x-ray diffraction mesurments. The modulus of elasticity are calculated as $c_{11}=12.8529(1-x)+16.74x$, $c_{12}=4.826(1-x)+6.523x$, $c_{44}=6.68(1-x)+7.957x$. The expression for the deformation potential coupling constant is taken as d (meV)$=-5320x-5500(1-x)$. Band offset is accounted for by following Ref. 22. Accordingly, we have calculated the energy of the valence band in the QW and in the alloy as $E_v(x)$ (meV)$=[-20a$ (Å)$+236.2](1-x)/0.22+\Delta/3$, there Δ (meV)$=300-260x$ is the energy of the spin-orbit splitting. Then, the valence band offset is calculated from $E_v(x)-E_v(0)$.

The eigenfunctions of the Hamiltonian in Eq. (1) are computed in the vector potential gauge specified by $\vec{A}=1/2[\vec{H}\times\vec{r}]$ and using the axial approximation in which the nondiagonal terms proportional to $(\gamma_2-\gamma_3)$ (which is related to the anisotropy in the plane of the QW layer) are neglected.[17] This approximation is fully justified within a first order perturbation theory. In this case, the projection of the electron angular momentum on the OZ axis, J_z, is an integral of motion and the wave functions of the basis states have the form

$$\vec{\Psi}^M_{i,n}(\rho,\theta,z)=\begin{Bmatrix} f_4^{i,n}(z)u_{n-3,M-3}(\rho,\theta) \\ f_3^{i,n}(z)u_{n-2,M-2}(\rho,\theta) \\ f_2^{i,n}(z)u_{n-1,M-1}(\rho,\theta) \\ f_1^{i,n}(z)u_{n,M}(\rho,\theta) \end{Bmatrix}. \tag{4}$$

Each of the basic states is characterized by a quantum number n $(n=r+[|M|+M]/2,\ r=0,1,\ldots,\infty,$ with $M=J_z/\hbar+3/2)$ labeling the Landau level, by a wave function parity with respect to the plane XOY, and by the index i which labels the levels of size quantization; θ is the angle in the XOY plane; $f_j^i(z)$ are functions to be defined on z; $u_{n,M}$ is the normalized Landau wave function[23]

$$u_{n,M}(\rho,\theta)=\frac{1}{\lambda}\sqrt{\frac{r!}{(r+|M|)!}}\frac{\exp(iM\theta)}{\sqrt{2\pi}}x^{|M|/2}$$

$$\times\exp(-x/2)L_r^{|M|}(x), x=\frac{\rho^2}{2\lambda^2}, \tag{5}$$

where ρ is the radius in cylindrical coordinates and $L_r^{|M|}(x)$ are the Laguerre polynomials.[24] In the vector-potential gauge used here, the creation and annihilation operators are represented as

$$\hat{a}^{\pm}=-\frac{i}{\sqrt{2}}\exp(\pm i\theta)\left[\lambda\frac{\partial}{\partial\rho}\pm i\left(\frac{\lambda}{\rho}\frac{\partial}{\partial\theta}+i\frac{\rho}{\lambda}\right)\right],$$

$$\hat{a}^{+}|u_{n,M}\rangle=i\sqrt{n+1}\times\mathrm{sgn}(M)|u_{n+1,M+1}\rangle,$$

$$\hat{a}^{-}|u_{n,M}\rangle=-i\sqrt{n}\times\mathrm{sgn}(M-1)|u_{n-1,M-1}\rangle. \tag{6}$$

Here $\mathrm{sgn}(M)$ is equal to 1 if $M\geqslant 0$ or to -1 if $M<0$. The Landau states are infinitely degenerate with respect to M, such that $M=-\infty,\ldots,-1,0,\ldots,n$. The equations obtained by substituting Eq. (4) into Eq. (1) are solved using the transfer-matrix technique,[25] and assuming an exponential decay of $f_j^i\{j=1,\ldots,4\}$ in the barriers.

Since n cannot be negative, appropriate components of the function $\vec{\Psi}^M_{i,n}$ should be set equal to 0. Thus, only a component containing $f_1^i(z)$ for $n=0$ is different from zero, and it is necessary to solve only one differential equation to find the wave function. For $n=1$ and $n=2$ the problem of finding the basis functions is reduced to solve two and three differential equations, respectively. For $n>2$ the same problem is reduced to solve four differential equations.

Here we are interested in the impurity states whose wave functions are localized in the QW regardless of the position of the impurity inside the HS. For such states we may neglect the wave functions of the continuous spectrum above the barrier, which constitute a part of the complete set of basis functions, and write the acceptor wave function as

$$\vec{\varphi}^M(\rho,\theta,z)=\sum_{i=1}^{i_{\max}}\sum_{n=[|M|+M]/2}^{n_{\max}}c^M_{i,n}\vec{\Psi}^M_{i,n}(\rho,\theta,z). \tag{7}$$

The expansion coefficients $c^M_{i,n}$ are rapidly decreasing at increasing i and n. Therefore, we may truncate the series at some $n_{\max}$ and $i_{\max}$. These maximum numbers are chosen from the condition that the energy of the last state which is taken into account in the expansion should be much higher than that of the acceptor ionization (i.e., $n_{\max}\gg[\lambda/a_B]^2$, with a_B the Bohr radius of the impurity, and $i_{\max}\gg[d_{\mathrm{Ge}}/a_B]^2$, where d_{Ge} is the QW width). In the matrix representation the solution of the Schroedinger equation is reduced to the diagonalization of a Hermitian matrix $\|D\|$ with elements

$$D^M_{i1,i2,n1,n2}=\delta^{i1,i2}_{n1,n2}E^M_{i1,n1}-e^2/\epsilon_r$$
$$\times\sum_{l=1}^{4}\int_0^{2\pi}\int_{-\infty}^{\infty}\int_0^{\infty}\frac{u_{n1-l,M-l}f_l^{i1,n1}u_{n2-l,M-l}(f_l^{i2,n2})^*}{\sqrt{\rho^2+(z-z_i)^2}}$$
$$\times\rho d\rho dz d\theta, \tag{8}$$

where ϵ_r is the relative refraction coefficient of Ge, $E^M_{i1,n1}$ are the energies of the basis states, z_i is the coordinate defining the location of an impurity atom as measured from the center of the QW. The number $n_{\max}$ grows at reducing the magnetic field, and the dimension of the matrix $\|D\|$ is increased simultaneously. The increased complexity of calculations makes the present method not appealing to be used in a weak magnetic field ($H<10$ kOe in our case).

The interaction of the electromagnetic radiation with an electron can be described by introducing an electric field E from a scalar potential as $\varphi=-\vec{E}\cdot\vec{r}$. Let us consider a circular polarized wave in which the electric field vector rotates in the same direction as that of the electron in a magnetic field. In this case the scalar potential takes the form

$$\varphi = -E(x+iy)\exp(-i\omega t) - E(x-iy)\exp(i\omega t) \quad (9)$$

with ω the circular frequency. The first sum on the right-hand side of Eq. (9) describes the process of photon absorption, and the second one that of photon emission. Accordingly, the process of absorption is determined by a matrix element of the operator $\hat{x}^+ = \hat{x} + i\hat{y}$ and the process of emission by that of the operator $\hat{x}^- = \hat{x} - i\hat{y}$ (the meanings of these operators are interchanged in the case of the opposite polarization). The matrix elements of optical transitions between different acceptor states $|\vec{\varphi}_s^{M_s}(\rho,\theta,z)\rangle$ and $|\vec{\varphi}_t^{M_t}(\rho,\theta,z)\rangle$ are calculated using Eqs. (4)–(7). Accordingly, we have obtained

$$\langle \vec{\varphi}_s^{M_s} | \hat{x}^{\pm} | \vec{\varphi}_t^{M_t} \rangle = \sum_{i_t=1}^{i_{\max}} \sum_{i_s=1}^{i_{\max}} \sum_{\substack{n_t=[|M_t|\\ +M_t]/2}}^{n_{\max}} \sum_{\substack{n_s=[|M_s|\\ +M_s]/2}}^{n_{\max}} c_{i_s,n_s}^{M_s} (c_{i_t,n_t}^{M_t})^* \times \int_0^{2\pi} \int_{-\infty}^{\infty} \int_0^{\infty} \vec{\Psi}_{i_s,n_s}^{M_s} \hat{x}^{\pm} (\vec{\Psi}_{i_t,n_t}^{M_t})^* \rho d\rho dz d\theta, \quad (10)$$

where

$$\begin{aligned} &\int_0^{2\pi} \int_{-\infty}^{\infty} \int_0^{\infty} \vec{\Psi}_{i_s,n_s}^{M_s} \hat{x}^{\pm} (\vec{\Psi}_{i_t,n_t}^{M_t})^* \rho d\rho dz d\theta \\ &= \sum_{l=1}^{4} \int_{-\infty}^{\infty} f_l^{i_s,n_s}(z) [f_l^{i_t,n_t}(z)]^* dz \\ &\quad \times \int_0^{2\pi} \int_0^{\infty} u_{n_s-l,M_s-l}(\rho,\theta) \hat{x}^{\pm} u_{n_t-l,M_t-l}(\rho,\theta) \rho d\rho d\theta \\ &= \sum_{l=1}^{4} \int_{-\infty}^{\infty} f_l^{i_s,n_s}(z) \\ &\quad \times [f_l^{i_t,n_t}(z)]^* dz \langle u_{n_s-l,M_s-l}(\rho,\theta) | \hat{x}^{\pm} | u_{n_t-l,M_t-l}(\rho,\theta) \rangle. \end{aligned} \quad (11)$$

Now, we look for the relation between the matrix elements of the operators $\hat{x}^+$ ($\hat{x}^-$) and $\hat{a}^+$ ($\hat{a}^-$) in the set of functions $\{u_{n,M} | n = 0,1,\ldots,\infty; M = -\infty,\ldots,n-1,n\}$. These matrix elements are obtained directly by using Eqs. (5) and (6). For the nondiagonal matrix elements it is

$$\begin{aligned} \langle u_{n+1,M+1} | \hat{x}^+ | u_{n,M} \rangle &= -i\lambda\sqrt{2} \langle u_{n+1,M+1} | \hat{a}^+ | u_{n,M} \rangle, \\ \langle u_{n,M} | \hat{x}^- | u_{n+1,M+1} \rangle &= i\lambda\sqrt{2} \langle u_{n,M} | \hat{a}^- | u_{n+1,M+1} \rangle. \end{aligned} \quad (12)$$

For the matrix elements diagonal with respect to n it is[2]

$$\begin{aligned} \langle u_{n,M+1} | \hat{x}^+ | u_{n,M} \rangle &= \langle u_{n,M} | \hat{x}^- | u_{n,M+1} \rangle \\ &= -\mathrm{sgn}(M)\sqrt{2}\lambda\sqrt{n-M}. \end{aligned} \quad (13)$$

All other matrix elements are equal to zero. Equations (12) and (13) reflect the fact that, owing to conservation of the angular momentum projection, optical dipole transitions in the Faraday configuration are allowed only when M (J_z) changes by unity ($\Delta M = \pm 1$). Thus, the resulting expressions for the matrix elements of optical dipole transitions are given by

$$\begin{aligned} &\langle \vec{\varphi}_s^{M+1} | x^+ | \vec{\varphi}_t^{M} \rangle \\ &= \sum_{i_t=1}^{i_{\max}} \sum_{i_s=1}^{i_{\max}} \sum_{\substack{n_t=[|M|\\ +M]/2}}^{n_{\max}} \sum_{\substack{n_s=[|M+1|\\ +M+1]/2}}^{n_{\max}} c_{i_s,n_s}^{M+1} (c_{i_t,n_t}^{M})^* \\ &\quad \times \mathrm{sgn}(M)\lambda\sqrt{2} \\ &\quad \times \sum_{l=1}^{4} \left[\delta_{n_s,n_t+1} \sqrt{n_t - l} \int_{-\infty}^{\infty} f_l^{i_s,n_s} (f_l^{i_t,n_t})^* dz \right. \\ &\quad \left. - \delta_{n_s,n_t} \sqrt{n_t - M} \int_{-\infty}^{\infty} f_l^{i_s,n_s} (f_l^{i_t,n_t})^* dz \right] \end{aligned} \quad (14a)$$

and

$$\begin{aligned} &\langle \vec{\varphi}_s^{M-1} | \hat{x}^+ | \vec{\varphi}_t^{M} \rangle \\ &= \sum_{i_t=1}^{i_{\max}} \sum_{i_s=1}^{i_{\max}} \sum_{\substack{n_t=[|M|\\ +M]/2}}^{n_{\max}} \sum_{\substack{n_s=[|M-1|\\ +M-1]/2}}^{n_{\max}} c_{i_s,n_s}^{M-1} (c_{i_t,n_t}^{M})^* \\ &\quad \times \mathrm{sgn}(M-1)\lambda\sqrt{2} \\ &\quad \times \sum_{l=1}^{4} \left[\delta_{n_s,n_t-1} \sqrt{n_s - l} \int_{-\infty}^{\infty} f_l^{i_s,n_s} (f_l^{i_t,n_t})^* dz \right. \\ &\quad \left. - \delta_{n_s,n_t} \sqrt{n_t - (M-1)} \int_{-\infty}^{\infty} f_l^{i_s,n_s} (f_l^{i_t,n_t})^* dz \right]. \end{aligned} \quad (14b)$$

In the above Eqs. (14a) and (14b) the expressions under the square roots must be positive, in the opposite case they are replaced by zero.

We note that the use of the matrix element of the velocity operator $\hat{\vec{V}}$ (gauge for the light wave $\varphi = 0$, $\vec{A} = icE/\omega$)[26] provides the same results as for the case when use is made of the matrix element of the position operator $\hat{\vec{r}}$ [see Eq. (16) of Sec. III B] for the calculation of the hole transition probability due to light absorption. Indeed, by recalling the well known relation

$$\vec{V}_{st} = \frac{d\hat{\vec{r}}_{\mathrm{st}}}{dt} = \left(\frac{\partial \hat{H}}{\partial \vec{k}} \right)_{st} = \frac{i}{\hbar} [\hat{H}\hat{\vec{r}}]_{st} = \frac{i}{\hbar} (E_s - E_t) \vec{r}_{st}$$

and taking into account energy conservation ($\hbar\omega = E_t - E_s$), one obtains the same result for both representations. However, when calculating the photoresponse, the use of the position representation is more adequate, because it gives physically sound results in the low-frequency limit $\omega \to 0$. Indeed, the use of the velocity operator for the photoresponse (photoabsorption) calculation has the drawback of leading to an infinite value for $\omega \to 0$.[27] This fact is due to the incorrect use of perturbation theory in the gauge $\varphi = 0$, $\vec{A} = icE/\omega$ for ω tending to zero. We stress that the use we made here of the position representation has the advantage of overcoming this

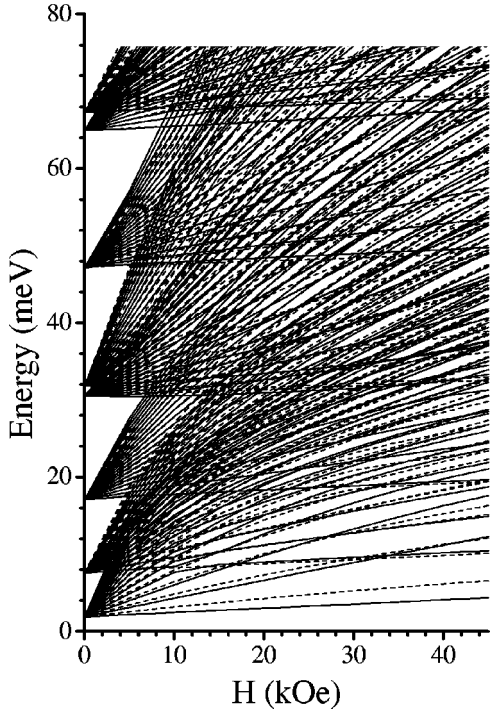

FIG. 1. Fan chart of the calculated basis state energies as a function of the magnetic field. Here and in all other figures the energy is referred to holes and thus the energy axis is directed upward. Solid and dashed lines correspond to the states with the wave functions, respectively, of even and odd parity with respect to the XOY plane.

drawback by providing a photoresponse value which tends to zero in the limit of vanishing frequency when $\omega \to 0$.

III. RESULTS AND DISCUSSION

In the following we present the results concerning the acceptor states in the elementary cell of the HS and then these results are applied to model the spectra of the photoresponse of the whole HS. Calculations are specialized for a structure where the photoresponse was measured in the presence of a magnetic field.[14]

A. Acceptor states

Calculations are performed for the $Ge/Ge_{0.88}Si_{0.12}(111)$ multilayer HS No. 306 ($d_{Ge} \simeq d_{GeSi} \simeq 200$ Å, number of periods 162) containing quantum wells in the strained layers of Ge ($\varepsilon_{xx} = 2.1 \times 10^{-3}$). Residual acceptors with a concentration of the order of 10^{14} cm^{-3} were found in this undoped HS.[14] In the present calculations n_{max} is taken equal to 30 and i_{max}, representing the double number of size quantization levels in the QW, is taken at most equal to 16.

Figure 1 shows the fan charts of the calculated basis states, which are essentially Landau states, at different energies as a function of the magnetic field. At zero magnetic field, all states collapse on the 8 subband of size quantization. The fourth subband of size quantization in Fig. 1 (at 30.5 meV) corresponds to the light hole subband. In each fan chart related to the size qantization subband there are two

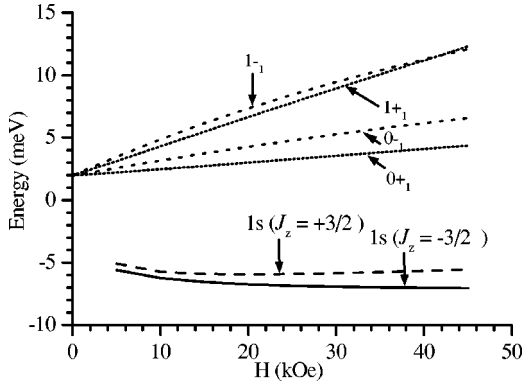

FIG. 2. Two lowest $1s$-like states referred as $J_z = -(3/2)\hbar$ (solid lines) and $J_z = +(3/2)\hbar$ (dashed lines) for the acceptor located in the center of the QW versus the magnetic field. The four higher energy states refer to the fan chart of the lowest Landau levels of free holes in the QW. For the notations used see the text.

different groups of states with corresponding wave functions of even (solid lines) and odd (dashed lines) parity with respect to the XOY plane. Let us classify these states as $N \pm_i$. Here $+$ or $-$ designates the wave function parity with respect to the XOY plane, i labels the size quantization subband, N and numbers the state in each group of states with the same parity in each subband with respect to the energy increase ($N = 0,1, \ldots, \infty$). The first state at the lowest energy in Fig. 1 is the state of even parity and has a dominant envelop function component f_4. This component corresponds to the Bloch function $\psi^{3/2}_{-3/2} = (|X\downarrow\rangle - i|Y\downarrow\rangle)/\sqrt{2}$,[18] i.e., to heavy hole (hh$\downarrow$) subband with effective spin antiparallel with the magnetic field direction. We mark this state as $0+_1$. The second state at higher energy $0-_1$ (dashed line) is connected with the Bloch function $\psi^{3/2}_{+3/2} = (|X\uparrow\rangle + i|Y\uparrow\rangle)/\sqrt{2}$ and has the f_1 as a dominant component of the envelope function. This state represents the zero Landau level in the heavy hole subband with the spin oriented parallel with magnetic field (hh$\uparrow$). The acceptor ground state in the above structure is twofold degenerate. The magnetic field splits the ground state into two states with different values of J_z.

Figure 2 reports the splitted ground states of an acceptor located in the center of the QW. The continuous curve corresponds to $J_z = -(3/2)\hbar$, and the dashed curve is related to $J_z = (3/2)\hbar$. Such an acceptor location preserves the symmetry of the system and the acceptor wave function parity is a ''good'' quantum number. Therefore, the lowest acceptor state in Fig. 2 is related only to the $N+_i$ basis states and the acceptor state with $J_z = (3/2)\hbar$ is connected only with $N-_i$ basis states. The lowest Landau levels in the first subband of size quantization of the free holes are reported by the dotted curves in Fig. 2. The rare dots represent the $N-_0$ and $N-_1$ Landau levels. We note, that the two acceptor ground states, which binding energies systematically increase with magnetic field, exhibit an energy splitting similar to that of the two $N=0$ Landau levels. We consider further optical transitions only from the lowest acceptor state with J_z

$=-(3/2)\hbar$ $(M=0)$ since the higher state [with $J_z=(3/2)\hbar$] is not populated at $T=4.2$ K, the temperature used in Ref. 14.

In the limit of high magnetic fields, when the magnetic length is comparable with the localization radius of the impurity state, the wave function of the acceptor state is mostly determined by the magnetic field[11,13,28] and is similar to the wave function belonging to one of the M degenerate states corresponding to the Nth Landau level from which this acceptor state is formed.

Figure 3 reports the energies of the excited states for an acceptor located at the center of the QW calculated with $M=\pm 1$, respectively, Figs. 3(a) and 3(b), to which optical transitions from the ground state are allowed. Since we consider intermediate magnetic fields, it is difficult to classify unambiguously these states in terms of low- or high-field limits. Indeed, the physical picture is neither high-field Landau-like nor low-field hydrogenlike. Since the energy separation between basis states is less than or comparable to the ionization energy, acceptor states are formed by many basis states. Let us name the ground state a $1s$ state and the lowest excited states in Figs. 3(a) and 3(b) as $2p_{-1}$ and $2p_{+1}$ states, respectively. This notation could be justified by the fact that the dominant component of the four component envelope function of these states has the same symmetry as the wave functions of the above states in the case of donors.[29–33] The insets in Fig. 3 report the dimensionless matrix elements for optical transitions $(\langle|\hat{x}^{\pm}|\rangle/\sqrt{2}\lambda)$ related to transitions from the ground to the excited states labeled with different numbers. As expected, we found that the optical transitions $1s\rightarrow 2p_{\pm 1}$ are dominant, and their matrix elements become the most relevant ones in high magnetic field, where the number N of a Landau level becomes a good quantum number. Furthermore, at high fields and in the given Faraday configuration the dominant transitions are those with $\Delta N=\pm 1$ and $\Delta N=0$ between the states with the same parity.

Figure 4(a) reports the acceptor energy states $1s$, $2p_{\pm 1}$ and the forth upper state as a function of the magnetic field for the impurity ion located in the QW center (solid line) and in the QB center (dashed lines). As expected, the energy of the $2p_{+1}$ state increases linearly with magnetic field until it anticrosses with the forth upper state. When moving from the center of the QW to the center of the QB, the ground state becomes significantly more shallow, and the energy of the excited states increases systematically to a lower extent. Figure 4(b) reports the dimensionless matrix elements of the transitions $1s\rightarrow 2p_{-1}$, $1s\rightarrow 2p_{+1}$ and from the $1s$ to the forth upper state for an acceptor located at the center of QW. Here the first two matrix elements proved to behave in a very similar way systematically increasing up to a magnetic field value of about 40 kOe. Then, the second matrix element starts decreasing significantly by crossing the third matrix element because of the anticrossing behavior of the corresponding energy states related to different subbands. In any case, in the limit of high magnetic fields we find that the $1s\rightarrow 2p_{-1}$ and $1s\rightarrow 2p_{+1}$ transitions matrix elements have a tendency to approach unity. All other transitions from the

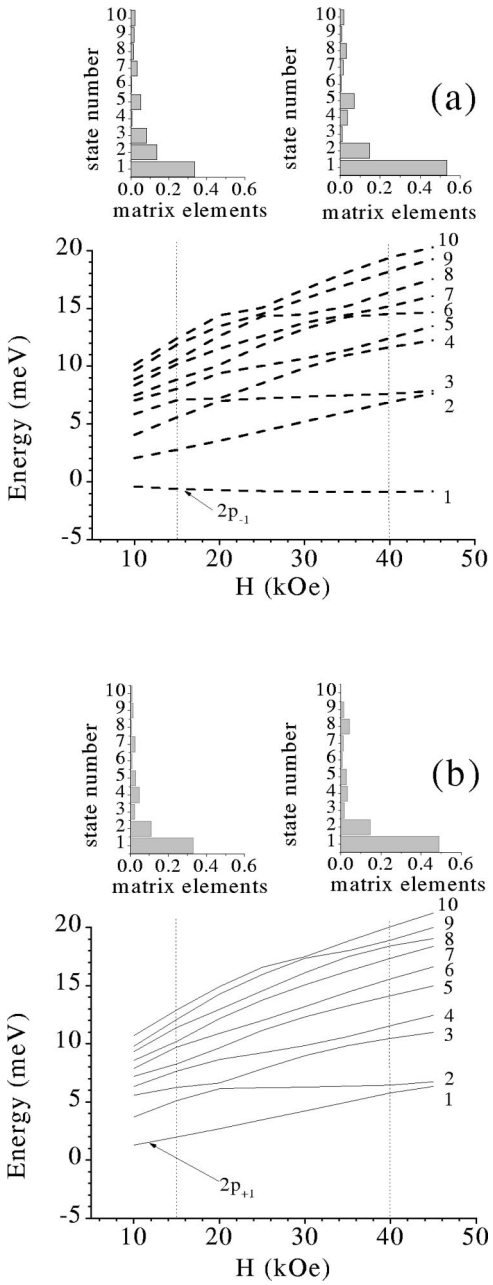

FIG. 3. Series of calculated excited states with, respectively, (a) $M=-1$ and (b) $M=+1$ bound to an acceptor ion located in the center of the QW versus the magnetic field. The insets show the amplitudes of the dimensionless matrix elements $\langle i|\hat{x}^{\pm}|f\rangle/\sqrt{2}\lambda$ associated with optical transitions from the ground state $(1s)$ to the labeled state at the given magnetic field intensity.

ground state to the states bound to the Landau levels in the first subband of the size quantization are characterized by matrix elements tending to zero. Due to a reduced localization of the wave function in the Coulomb potential of an impurity located at the barrier, the properties of an impurity located in center of the QB are found to reach the asymptotic values of the high magnetic field earlier than those of an impurity located in the center of the QW. For the case $H=40$ kOe, the dimensionless matrix elements $(\langle 1s|\hat{x}^{\pm}|2p_{\pm 1}\rangle/\sqrt{2}\lambda)$ corresponding to the basic transitions

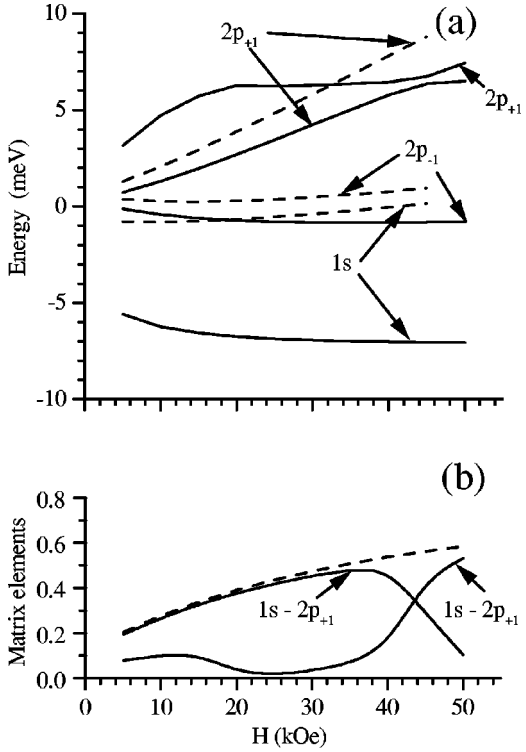

FIG. 4. (a) Acceptor energies states versus the magnetic field in the Ge/GeSi HS No. 306 of Ref. 14. Calculations refer to an acceptor located in the center of the QW (solid lines) and in the center of the QB (dashed lines). (b) Amplitudes of the matrix elements for optical transitions from the ground state to the $2p_{-1}$ (dashed line) and to the $2p_{+1}$ and the higher state (solid lines), respectively, versus the magnetic field for an acceptor located in the center of the QW.

$1s \rightarrow 2p_{+1}$ and $1s \rightarrow 2p_{-1}$ for an acceptor centered at the barrier also tend to unity and reach practically the value of 0.8 (to be compared with the value of 0.5 for the center of the quantum well). In this system there is also the possibility for transitions to higher excited states belonging to the second and third subbands.

However, in the present case the corresponding matrix elements are found to be negligibly small. Our interest to the location of acceptors at the high symmetric points, such as the center of the QW and that of the QB, is now extended to all the intermediate points, as shown in Fig. 5. Here the energy levels of the $1s$ ground state and the first two excited p states are reported as a function of the acceptor position inside the elementary cell of the HS for $H=50$ kOe. Furthermore, for reason of completeness Fig. 5 also shows the positions of the lowest Landau levels of free holes in the QW. As expected, the ground state energy is found to become two times closer to the bottom of the valence band (i.e., to the lowest Landau level) when the acceptor moves from the center of the QW to that of the QB while the excited states positions do not change so significantly. From Fig. 5 we notice, that the ionization energy [here denoted as the difference between the ground impurity state and the bottom of the lowest free (2D) hole subband in the QW in the absence of an impurity] tends to zero when the impurity ion

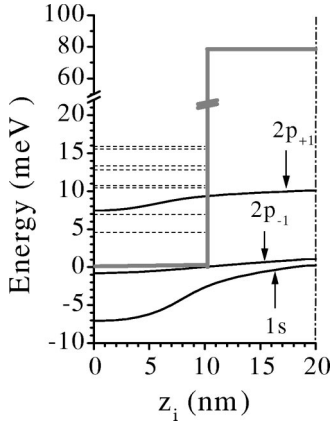

FIG. 5. Acceptor state energies (continuous lines) and Landau states of free holes (dotted lines) as a function of the acceptor position inside the elementary cell of a HS for a magnetic field $H=50$ kOe. The zero of the energy is taken to coincide with the bottom of the valence band for heavy holes in pure Ge.

is placed in the barrier far from the heterointerface. In other words, if the QW is deeper than the impurity binding energy in the bulk material then the ground state of both the impurity located at the well and the impurity located at the barrier is always formed by the hole wave functions in the QW rather than those in the bulk even if the impurity is located far in the barrier (in the last case the impurity ion located at the barrier binds the hole in the QW). This fact is well known and has been discussed in the literature.[1] Furthermore, the effect of the quantum confinement on the acceptor binding energy in unstrained QW is dual. From one hand the confinement implies an increase of the binding energy due to the additional localization of the acceptor wave function near the impurity ion (just as in the case of donors). However, from another hand the confinement leads to the splitting of the valence band thus decreasing the hole effective mass and the acceptor binding energy. According to present calculations, in an unstrained Ge QW of 200 Å width, these two effects just compensate each other.

Figure 6 reports the dimensionless square matrix elements of optical transitions from the ground state to all the excited states as a function of the transition energy for $H=40$ kOe (a) and for $H=15$ kOe (b), respectively. With the purpose of modeling a uniform impurity distribution, the square matrix elements are calculated in 20 equidistant layers starting from the center of the QB and ending at the center of the QW, thus sampling the whole elementary cell of Fig. 5. We note that a first group of lines in Fig. 6(a) covers the range of energies from about 1 to 6 meV. They refer to transitions from the $1s$ ground state to the $2p_{-1}$ excited state and their magnitude decreases systematically in going from the center of the QB (labeled as line 0 in the figure) to the center of the QW (labeled as line 1). This dependence reflects the fact that the wave functions of acceptor states becomes more localized in the XOY plane when the impurity is located in the center of the QW. This fact reduces the functions overlap in the integral determining the transition matrix element when going from the center of the QB to that of the QW. Furthermore, the lines are denser near to the extremes. A second group of

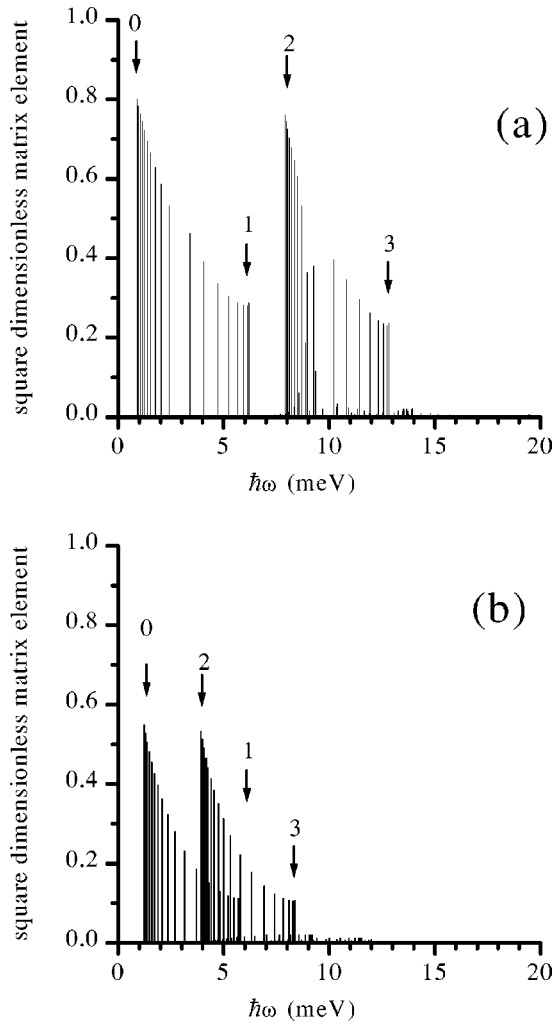

FIG. 6. Oscillator strength as a function of the transition energy from the ground state to all excited states for a magnetic field $H=40$ kOe (a) and $H=15$ kOe (b). We consider all optical transitions which are allowed and with energies up to 20 meV for all layers (with step 1 nm) in the HS period of Fig. 5.

lines in Fig. 6(a) covers the range of energies from about 8 to 13 meV. They refer to transitions $1s\rightarrow 2p_{+1}$. The left-hand side of this band (labeled as line 2) corresponds to the transition energy between states of acceptor located in the center of the QB and the right hand side (labeled as line 3) corresponds to the acceptor in the center of the QW. In this band there is a secondary maximum at an energy of about 10 meV which is associated with the anticrossing exhibited by the $2p_{+1}$ and the next higher level. The lines concentrate at transition energies for acceptors situated near the centers of both the QW and the QB. Furthermore, there are some tails of lines evidencing some small contributions associated with transitions from the $1s$ ground state to higher excited states not reported in Fig. 5. If we suppose that the acceptor is located only in the center of the QW, then we would obtain only the two peaks labeled as 1 and 3. By contrast, if the acceptor is located only in the center of the QB we would obtain only the two peaks labeled as 0 and 2. A distributed location of the acceptors implies the existence of four peaks. We note that a uniform distribution and an equally concentrated distribution at the two symmetric centers gives practically the same main features for the photoresponse spectra, because of the increase of the line density near the four peaks corresponding to the symmetric centers in case of the uniform distribution. In the case of a low magnetic field, as reported in Fig. 6(b), we note the natural tendency of the peaks labeled as 2 and 3 to overlap with the peaks labeled as 0 and 1.

B. Photoresponse

In the absence of a magnetic field, charge transfer in the plane of the quantum well occurs in subbands of size quantization. The presence of a magnetic field gives rise to Landau levels in each subband. With the gauge used here, the Landau levels are infinitely degenerate with respect to M (J_z), and the set of wave functions for each level can be used to form a propagating solution. The Coulomb potential of the impurity center breaks this degeneracy. Since the characteristic size of the localized state increases with increasing $|M|$, the states that are mostly shifted in energy are those with a small $|M|$ [we find that the electron occupying the acceptor ground state has $M=0$, i.e. $J_z=-(3/2)\hbar$]. The states with high values of $|M|$ are practically not changed by the Coulomb potential and remaining infinitely degenerate they control charge transfer in the presence of a magnetic field. As mentioned above, according to the selection rules, the optical transitions between the impurity states in the Faraday configuration are allowed only with $\Delta M=\pm 1$ for both right and left polarized radiation. Therefore, the transitions from the acceptor ground state directly into the continuum (formed by states with high values of $|M|$ originating from the Landau levels in the presence of an impurity) are forbidden. After photon absorption, an electron bound up with the acceptor ground state turns into the exited state. However, the presence of an electric field (Pool-Frenkel effect, impact ionization of excited states, etc.[34]) or a multiple absorption of acoustic phonons are likely to ionize an acceptor from the excited state, what ensures a charge transfer. In this case the surface concentration of free holes generated per unit time is

$$I_{hg}=n_i\sum_t P_t W_{s\rightarrow t}(f_s-f_t), \tag{15}$$

where n_i is the in plane impurity surface concentration of the considered layer and P_t is the ionization probability of the excited state

$|t\rangle$, f_s, and f_t are the occupation factors of the ground and excited states, respectively, $W_{s\rightarrow t}$ is the transition probability per unit time between the ground state $|s\rangle$ and the excited state $|t\rangle$ decribed by the Hamiltonian in Eq. (1) with eigenstates E_s and E_t, and given by Fermy golden rule

$$W_{s\rightarrow t}=\frac{2\pi(eE)^2}{\hbar}|\langle s|\hat{x}^{\pm}|t\rangle|^2\times\delta(E_s-E_t+\hbar\omega). \tag{16}$$

The photoresponse $J(\omega)$, which represents the total current through the HS, is proportional to I_{hg} and is expressed as

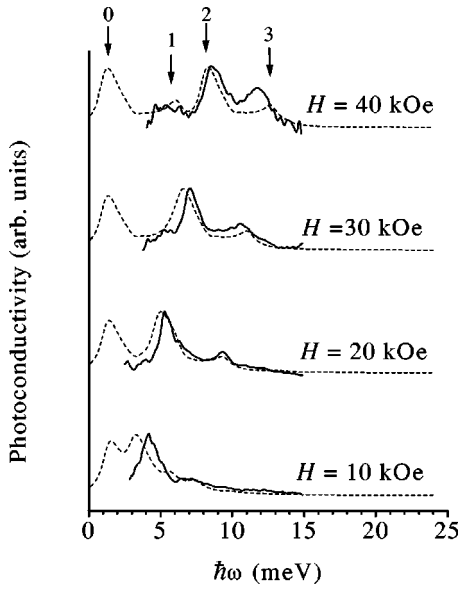

FIG. 7. FIR photoconductivity spectra of the undoped $Ge/Ge_{0.88}Si_{0.12}$ (111) sample No. 306 at different values of magnetic fields as reported in Ref. 14 with a residual acceptor concentration of the order of 10^{14} cm^{-3} (solid lines). Measurements were performed in the far-IR range at $T=4.2$ K with a BOMEM DA3.36 Fourier-transform spectrometer in the Faraday configuration ($\vec{k}\|\vec{H}$, $\vec{E}_\omega\perp\vec{H}$). A lateral dc electric field of 2–3 V/cm (below the impact ionization threshold) was applied to the sample. Arrows 0, 1, 2, and 3 designate the peaks in the spectra associated with the peaks of the oscillators strength lines in Fig. 6. Dashed curves are the photoconductivity spectra calculated from Eq. (14) of the text. Both the experimental and theoretical values of each spectrum are normalized to the maximum value.

$$J(\omega)\propto\int_{d_{\mathrm{Ge}}+d_{\mathrm{GeSi}}}\sum_t P_t(f_s-f_t)\langle s|\hat{x}^{\pm}|t\rangle|^2 \times\frac{E_L}{(E_s-E_t+\hbar\omega)^2+(E_L/2)^2}dz_i. \qquad (17)$$

Here the integral is taken over the elementary cell of the structure (see Fig. 5) and the δ function in Eq. (13) is replaced by a Lorentzian broadening (with $E_L=1$ meV) with the same phenomenological line width for all the transitions. To simplify the calculations, and in the absence of an exact knowledge of the ionization mechanism, we assumed, that $P_t\simeq 1$ for all the excited states. Also we assume a uniform distribution of impurity over the HS.

The quantity on the right-hand side (RHS) of Eq. (14) is calculated using the matrix elements reported in Fig. 6 and the obtained spectrum is normalized to its maximum value to be compared with experiments.

Figure 7 reports four typical spectra of the measured photoconductivity at different magnetic fields taken from Ref. 14 (solid lines) together with present theoretical calculations (dashed lines). For the convenience of comparison with the theory, the experimental curves are normalized to their maximum value. The impurity photoconductivity spectra in the far-IR range were measured at $T=4.2$ K with an applied

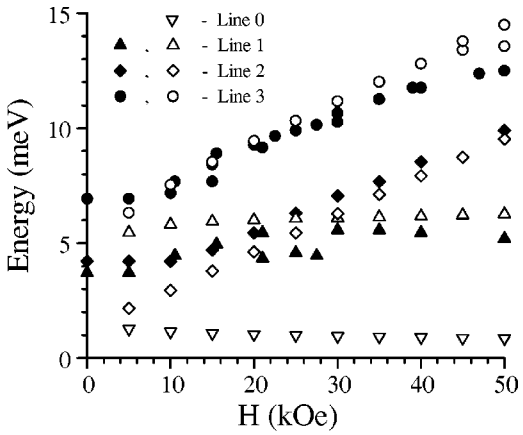

FIG. 8. Spectral positions of the photoconductivity peaks as observed experimentally (full symbols) and calculated theoretically (open symbols) as a function of the magnetic field. The meaning of the different symbols is as follows: ○: $1s\rightarrow 2p_{+1}$ transition between acceptor states located in the center of the QB identified as line 3; Δ: $1s\rightarrow 2p_{+1}$ transition between acceptor states located at the center of the QB identified as line 2; ◇: $1s\rightarrow 2p_{-1}$ transitions between acceptor states located in the center of the QW identified as line 1; and ∇: $1s\rightarrow 2p_{-1}$ transitions between acceptor states located in the center of the QB identified as line 0 (this line is outside the spectral range of the experimental apparatus).

electric field of 2–3 V/cm at constant magnetic fields using a BOMEM DA3.36 Fourier-transform spectrometer. The magnetic field was applied along the HS axis, and the measurements were made in the Faraday configuration ($\vec{k}\|\vec{H}$, $\vec{E}_\omega\perp\vec{H}$). The experimental spectra were found to exhibit three peaks labeled, respectively, as 1, 2, and 3 in the figure. Peak 1 shows to be practically independent of the magnetic field and to merge with peak 2 at lowering the magnetic field.

Peaks 2 and 3 exhibit linear blueshifts with the increase of the magnetic field. A forth peak, labeled as 0 in the figure, is predicted theoretically but at energies corresponding to frequencues below the experimental low limit. The measured photoconductivity spectrum and the magnetic field behavior of different peaks can be interpreted on the basis of the energy spectrum and wave functions of the acceptor centers as reported in the following. The spectra in Fig. 7 are just obtained from the data given in Fig. 6 with a fitting broadening factor of 1 meV which accounts for some phenomenological linewidth. The sharp transition peaks in Fig. 7 is mostly a consequence of the singularity of the density of states which takes place at the symmetric points, such as the centers of the QW and QB. In particular, from the results of Fig. 6, the lines 1 and 3 are associated with the energy levels of the acceptor located in the center of the QW, while the lines 0 and 2 are associated with the acceptors located at the center of the QB. The general features of the experiments are reproduced by theory. In any case, the position of the peaks and their broadening is still subjected to minor quantitative improvements.

For a more detailed comparison between theory and experiments, Fig. 8 reports the energy position of different peaks as a function of the magnetic field. These positions are determined from the experimental photoconductivity spectra

and from the calculated ones. By focusing on the region of magnetic fields above 10 kOe, where the theory is better suited for the microscopic interpretation, the experiments are found to be reproduced within an uncertainty of at most 20%. We note that, at the highest magnetic fields, the calculated line 3 obtains contributions from different excited states because of the anticrossing exhibited by the third and upper excited levels. Accordingly, at 45 and 50 kOe, we have reported the two contributions in Fig. 8. The comparison between the theory and experiments is considered to be satisfactory. Theoretical findings support the qualitative interpretation given above and confirm that lines 1 and 3 correspond to transitions $1s \rightarrow 2p_{-1}$, $1s \rightarrow 2p_{+1}$ between states of acceptors located in the center of the QW. Furthermore, the peak associated with the line 2 is found to correspond to transitions such as $1s \rightarrow 2p_{+1}$ between the states of acceptor located in the center of the QB. The prediction of a line at a low energy of about 1 meV is waiting for an experimental confirmation. We finally remark, that at low magnetic fields ($H < 10$ kOe) the present theory still gives the correct values for the transition energies, but these depart from the experimental results for about 50% at most. The reason is that in small magnetic fields the dominant transitions are those from the ground-state to the continuum, and thus the photoconductivity line shifts to higher energies which are here not accounted for by theory. We remark that the experimental photoconductive spectra in the absence of the magnetic field were thoroughly interpreted using a complementary theoretical approach in Ref. 15.

The remaining disagreement between theory and experiments should be attributed to different sources. Among them the most probable can be as follows. (i) The deviation of the QW shape from the rectangular one, which can lead to a systematical underestimation of the values of the cyclotron mass needed to compute the basis functions. (ii) The neglect of central cell correction[35] in the model. (iii) The assumption made here of a uniform impurity distribution. (iv) The A^+ centers. We have not attempted to estimate the effects of these sources, which in any case are expected to be of minor importance. By contrast, we have estimated the effects of the coupling with the spin-orbit splitted band and of the anisotropy in the QW plane. We have found that by accounting for the spin-orbit splitted band the ground and the lowest excited acceptor states do not change noticeably. On the other hand, the effect of the anisotropy introduces corrections, which slightly (about 2–3 %) improve the agreement on the position of the third spectral peak.

IV. CONCLUSION

We have developed a microscopic theory for acceptor states in a quantum well of strained Ge/GeSi HS in the presence of both a deformation and a magnetic field. The location of the impurity atoms, when distributed between the center of the QW and the center of the QB, is found to originate a modulation of the acceptor energy states. Such a modulation is ultimately responsible for a photoconductance spectrum exhibiting several peaks whose position is in general function of the magnetic field. The comparison between theoretical calculations and experiments is found to be satisfactory thus enabling us to provide a microscopic interpretation of the relevant features of the experimental spectra. Further confirmation of present findings would require a direct control of doping position and density through direct experimental facilities which at present are not yet available.

ACKNOWLEDGMENTS

The work was supported by the RFBR (Grants Nos. 00-02-16568 and 01-02-16106), the Russian Leading Scientific Schools Support Grant No. 00-15-96618, the INTAS Grant No. YSF 00-60, and the Italian Ministry of Foreign Affairs through the Volta Landau Center (V.Ya.A.).

[1] G. Bastard, *Wave Mechanics Applied to Semiconductor Heterostructures* (Les Editions de Physique, Les Ulis, 1988).
[2] H. Hasegava and J. Howard, J. Phys. Chem. Solids **21**, 179 (1961).
[3] W. T. Masselink, Y.-C. Change, and H. Morkoc, Phys. Rev. B **32**, 5190 (1985).
[4] A. Pasquarello, L. C. Andreani, and R. Buczko, Phys. Rev. B **40**, 5602 (1989).
[5] J. P. Loehr, Y. C. Chen, D. Biswsas, P. K. Bhattacharya, and J. Singh, Phys. Rev. B **41**, 3695 (1990).
[6] S. Fraizzoli and A. Pasquarello, Phys. Rev. B **42**, 5349 (1990); **44**, 1118 (1991).
[7] G. T. Einevoll and Y.-C. Chang, Phys. Rev. B **41**, 1447 (1990).
[8] Q. X. Zhao and M. Willander, Phys. Rev. B **57**, 13 033 (1998); **62**, 5055 (2000).
[9] A. K. Ramdas and S. Rodriguez, Rep. Prog. Phys. **44**, 1297 (1981).
[10] W. Zawadzki, *Landau Level Spectroscopy*, edited by G. Landwehr and E. I. Rashba (Elsevier, Amsterdam, 1991).
[11] R. Chen, J. P. Cheng, D. L. Lin, Bruce D. McCombe, and Thomas F. George, J. Phys.: Condens. Matter **7**, 3577 (1995).
[12] Q. X. Zhao, P. O. Holtz, Alfredo Pasquarello, B. Monemar, and M. Willander, Phys. Rev. B **49**, 10 794 (1994); **50**, 2393 (1994); **63**, 195317 (2001).
[13] P. W. Barmby, J. L. Dunn, C. A. Bates, and T. O. Klaassen, Phys. Rev. B **57**, 9682 (1998).
[14] V. I. Gavrilenko, I. V. Erofeeva, A. L. Korotkov, Z. F. Krasil'nik, O. A. Kuznetsov, M. D. Moldavskaya, V. V. Nikonorov, and L. V. Paramonov, JETP Lett. **65**, 209 (1997).
[15] V. Ya. Aleshkin, B. A. Andreev, V. I. Gavrilenko, I. V. Erofeeva, D. V. Kozlov, and O. A. Kuznetsov, Semiconductors **34**, 563 (2000).
[16] L. K. Orlov, V. Ya. Aleshkin, N. G. Kalugin, N. A. Bekin, O. A. Kuznetsov, B. Dietrich, C. Bacquet, J. Leotin, M. Brousseau, and F. Hassen, J. Appl. Phys. **80**, 415 (1996).
[17] R. Winkler, M. Merkler, T. Darnhofer, and U. Rossler, Phys. Rev. B **53**, 10 858 (1996).

[18] G. L. Bir and G. E. Pikus, *Symmetry and Strain-Induced Effects in Semiconductors* (Wiley, New York, 1974).
[19] J. M. Luttinger, Phys. Rev. **102**, 1030 (1956).
[20] C. Martijn de Sterke, Phys. Rev. B **36**, 6574 (1987).
[21] G. Gagliani and L. Reggiani, Nuovo Cimento Soc. Ital. Fis., B **30**, 207 (1975).
[22] C. G. Van de Walle and R. M. Martin, Phys. Rev. B **34**, 5621 (1986).
[23] L. D. Landau and E. M. Lifshitz, *Quantum Mechanics (Non-relativistic Theory)*, 3rd ed. (Pergamon, New York, 1977).
[24] *Handbook of Matematical Functions*, Natl. Bur. Stand. Appl. Math. Ser. No. 55, edited by M. Abramovitz and I. A. Stegun (U.S. GPO, Washington, DC, 1964), p. 778.
[25] B. Ricco and M. Y. Azbel, Phys. Rev. B **29**, 1970 (1984).
[26] F. Szmolowicz, Phys. Rev. B **51**, 1613 (1995).
[27] B. W. Kim, E. Mao, and A. Majerfeld, J. Appl. Phys. **81**, 1883 (1997).
[28] J. L. Dunn and E. P. Pearl, J. Phys. C **3**, 8605 (1991).
[29] A. van Klarenbosch, T. O. Klaassen, W. Th. Wenckebach, and C. T. Foxon, J. Appl. Phys. **67**, 6323 (1990).
[30] D. Wintgen and H. Friedrich, J. Phys. B **19**, 991 (1986).
[31] R. J. Elliott and R. Loudon, J. Phys. Chem. Solids **15**, 196 (1960).
[32] W. S. Boyle and R. W. Howard, J. Phys. Chem. Solids **19**, 181 (1961).
[33] J. Simola and J. Virtamo, J. Phys. B **11**, 3309 (1978).
[34] L. Reggiani and V. Mitin, Riv. Nuovo Cimento **12**, 1 (1989).
[35] Sr. Gerardin Jayam and K. Navaneethakrishnan, J. Appl. Phys. **89**, 6198 (2001).